# Derivation of equivalent-linear impedance functions for pile-supported bridges from continuum model

Hooman Torabi, Mohammad T. Rayhani
*Department of Civil and environmental Engineering – Carleton University, Ottawa, Ontario, Canada*

ABSTRACT
Current equations for determination of pile head dynamic stiffness and damping for use in substructure analysis of soil-pile interaction are mostly based on linear elastic soil behavior and perfect contact at soil-pile interface. This paper presents application of a hybrid numerical-analytical methodology for equivalent-linear (EL) characterization of pile head impedance functions under inelastic soil-pile interaction. Inelastic continuum modeling, frequency-domain substructure formulation and closed-form derivation of impedance functions, based on Winkler assumption, are ingredients of the proposed approach. Results from three-dimensional (3D) nonlinear finite element (FE) analyses of single piles under dynamic pile head loading are used as input to the derivation algorithm. Variation of the computed impedances with pile head displacement is presented for the static and dynamic loading cases. The results indicate that gapping at the soil-pile interface and soil nonlinearity significantly reduce head impedances compared to the pile with rigid soil-pile connection. The results also demonstrate the capability of the proposed method in capturing the overall foundation damping, especially the vanishing radiation damping as the hysteretic damping prevails in the system.

## 1 INTRODUCTION

Pile foundations are extensively used to support various infrastructures such as bridges in soft soil where dynamic soil-structure interaction (SSI) can be of great importance for seismic resistant design (Mylonakis and Gazetas 2000). The substructure method is commonly used for the inertial SSI analysis of the bridge structures because of its remarkable computational efficiency, compared to the direct method by continuum models. Soil-pile interaction problem under immense inertial loads from superstructure, particularly in soft soils, is a nonlinear phenomenon. Hence, accurate quantification of its effect by the substructure method requires judicious characterization of the foundation impedance matrix as the key element of the substructure method to avoid conservative or unsafe design. These complex-valued frequency dependent functions represent dynamic stiffness and energy dissipation of dynamic interaction between near-field soil and foundation (Kausel et al. 1978).

In the current state of practice for SSI analysis (NIST 2012), the pile head impedance functions are estimated based on the viscoelastic soil behavior which has also been basis for majority of the previous studies on application of the substructure method for SSI analysis of bridge structures (e.g., Makris et al. 1994; Zhang and Makris 2002). The impedance functions used in this class of studies are based on outcomes of semi-analytical and numerical studies (Gazetas 1991) using combination of Winkler and finite element methods. The Winkler simplification of subgrade soil reaction in viscoelastic soil medium, which has been basis of analytical studies (Novak 1974; Mylonakis 1995), allows for tractable closed-form solution of soil-pile interaction in frequency-domain.

The generic p-y curves are widely used in practice to represent nonlinear soil-pile interaction and to determine the pile head impedances. Comparison of results from application of p-y curves with those from continuum models of soil-pile interaction demonstrates their unreliable performance particularly for predicting large pile deformation (McGann et al. 2011). Similar comparison showed that equivalent linearization of theses curves for use in nonlinear substructure analysis of bridges can be quite unreliable (Rahmani et al. 2016). While characteristics of the pile head impedance functions have been decently determined for linear soil-pile interaction, detailed mechanism and extent of inelastic interaction effects on the impedance function remain unclear. Characterization of these effects involves computation of impedances under load-dependent inelastic soil deformation and gap formation that is very likely to form at the pile-soil interface in cohesive soils under immense inertial loads.

This paper presents a hybrid approach for derivation of pile impedances from 3D continuum model of soil-pile interaction and representative results from its application to static and dynamic soil-pile interaction problems. In fact, this method is a back-calculating framework which combines the superiority and accuracy of the time-domain 3D continuum models in solving inelastic soil-structure interaction problem with computational convenience of the frequency-domain method and the practical Winkler-based impedance function formulation for piles.

## 2. Analysis Scheme

The hybrid approach devised in this study for characterization of the inelastic pile head impedance function consists of three components; each of which handles a specific aspect of the solution, totally different from the other two components. The solution algorithm is a back-calculating procedure in which the closed-form pile head impedance functions derived for a linear elastic beam on dynamic Winkler foundation (BDWF) are calibrated with results of the continuum models. In other words, coefficients of an equivalent homogenous bed of

viscoelastic Winkler elements (parallel spring and dashpot) supporting the pile shaft are interpolated by solving dynamic force-displacement equilibrium equations for a substructured pile in frequency domain. The elements of analytical-numerical approach and their contribution are described as follows:

2.1. Continuum model

Three-dimensional time-domain continuum modeling of soil-pile interaction system, a powerful numerical means of simulating fairly realistic nonlinear interaction phenomenon. By this technique, interaction between the inelastic soil and interface responses and radiation damping is rigorously captured. The continuum models of the soil-pile interaction for a single pile in a soft soil continuum are developed and subjected to static and dynamic loadings at the pile head in the OpenSees finite element (FE) program (McKenna and Fenves 2001). Hysteretic nonlinear stress-strain behavior of the saturated clayey soil is simulated using the total stress, pressure independent multi-yield surface constitutive model known as PIMY material in OpenSees. The 3D 8-node Brick element is used to discretize the soil domain. The elastic beam-column elements with three rotational and three translational degrees of freedom are used to model the pile shaft. Inelastic soil-pile interface behavior including slippage and gap openings under cyclic loads is simulated using the elasto-perfectly plastic interface material and 3D node-to-beam contact elements (Petek 2006). Cylindrical coordination is used for soil domain discretization as shown in Fig. 1 to enhance numerical convergence in presence of soil-pile interface elements and improve accuracy of interaction simulation. The concept of “sponge” boundary layer is used as a complementary measure to mimic the wave dissipation effect of unbounded soil domain following the procedure described by Varun et al. (2009). In this method, reflection of the waves back into the model is dissipated by high level of progressively increasing artificial damping assigned to the several outermost layers of soil element. This is implemented using the Rayleigh damping command in the OpenSees framework.

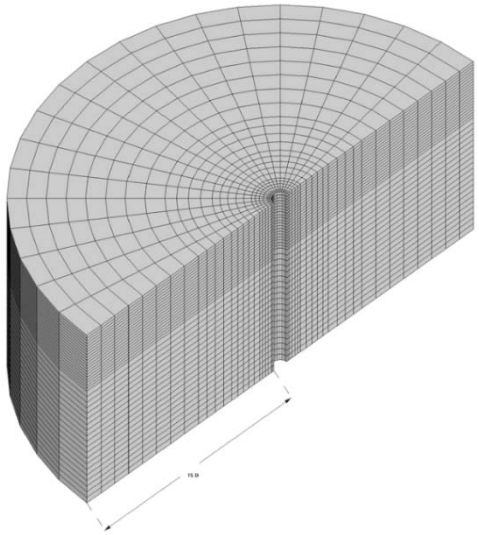

Figure 1. 3D continuum model of soil-pile interaction

2.2. Substructure formulation

The substructure formulation as the solution core is used as a simplifying tool for analysis of the inertial interaction. This method permits mathematical solution of the dynamic equation of motion using lumped dynamic resistance properties of underground soil-foundation system, including mass, stiffness and damping. In particular, the frequency-domain transform of the substructure formulation facilitates closed-form solution of the system response at a given loading frequency and amplitude. For a substructured model of pile shaft shown in Fig. 2, the pile response under a prescribed force at the pile head is described by the equation of motion in frequency domain as follows:

$$(-M\omega^2 + C\omega + K)\hat{U}(\omega) = \hat{F}_{ext}(\omega) \qquad [1]$$

where $S(\omega) = -M\omega^2 + C\omega + K$ is known as the complex-valued dynamic stiffness or impedance matrix of the underground system (Kausel et al. 1978; Wolf 1985), and “^ “ denotes the Fourier transform of the variables and U(t) denotes the displacement vector of the system. For a 2D analysis of a soil-pile interaction system using the substructure modeling approach, dynamic properties of the near-field soil medium and its interaction with the pile must be determined at the pile head, known as the pile head impedance functions. Replacing the system impedance with the equivalent pile head impedance for a 2D system in Eq. 2, the pile head response can be determined by solving:

$$\begin{bmatrix} S_{uu}(\omega) & S_{u\theta}(\omega) \\ S_{u\theta}(\omega) & S_{\theta\theta}(\omega) \end{bmatrix} \begin{bmatrix} \hat{u}(\omega) \\ \hat{\theta}(\omega) \end{bmatrix} = \begin{bmatrix} \hat{F}(\omega) \\ \hat{M}(\omega) \end{bmatrix} \qquad [2]$$

where $S_{uu}(\omega), S_{u\theta}(\omega)$ and $S_{\theta\theta}(\omega)$ represent the pile head impedances in the horizontal, cross-coupling and rocking vibration modes. The analytical procedure for derivation of the pile head impedances based on the Winkler model of soil-pile interaction and their alternative functional forms are presented in the following section.

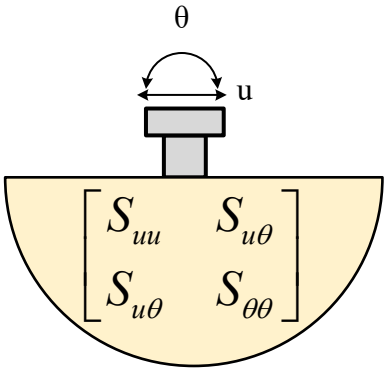


Figure 2. Substructure model of soil-pile interaction

2.3 Pile head impedance function

The third element of the hybrid solution involves analytical derivation of appropriate pile head impedance function in terms of polynomial functions which makes algebraic coupled solution for the system of equation of motions feasible for the pile cases of different boundary conditions. Elastodynamic solution of pile response under pile head moments and forces can be used to derive the pile head stiffness for elastic and equivalent-linear representation of nonlinear interaction problems. For a vertical pile foundation assumed as an Euler-Bernoulli beam, embedded in a homogeneous viscoelastic Winkler medium (Fig. 3), the pile response is determined by solving the governing equilibrium differential equation as follows:

$$E_p I_p \frac{\partial^4 u}{\partial z^4} + m_p \frac{\partial^2 u}{\partial t^2} + c\frac{\partial^2 u}{\partial t^2} + ku = 0 \quad [3]$$

where $E_pI_p$is flexural stiffness, $m_p$ is pile mass per length, and $u = u(z,t)$ is horizontal displacement of the pile. $k = k(z,\omega)$ and $c = c(z,\omega)$ denote frequency-dependent modulus of subgrade reaction and dashpot coefficients. The partial differential equation of Eq. 3 can be converted to an ordinary differential equation by assuming a harmonic steady state pile motion as follows:

$$u(z,t) = u(z)e^{i\omega t} \quad [4]$$

Substituting Eq. 4 into Eq. 3 yields to a simple ordinary differential equation:

$$\frac{\partial^4 u(z)}{\partial z^4} + \frac{(k + i\omega c - m\omega^2)}{E_p I_p} u(z) = 0 \quad [5]$$

where $K = k + i\omega c$ is the complex-valued impedance function of the Winkler medium. Solving the above equation for general and particular solutions yields to:

$$u(z) = e^{\lambda z}(A_1 \cos(\lambda z) + A_2 \sin(\lambda z)) + e^{-\lambda z}(A_3 \cos(\lambda z) + A_4 \sin(\lambda z)) \quad [6]$$

where $A_1$ to $A_4$ are solution constants and a characteristic parameter $\lambda$ is defined as below:

$$\lambda = \sqrt[4]{\frac{k + i\omega c - m\omega^2}{4E_p I_p}} \quad [7]$$

which is known as Winkler wavenumber that controls attenuation of the pile head excitation along the pile length, and its inverse from $(1/\lambda)$ which has a displacement unit called characteristic wavelength. The elastic soil-pile interaction stiffness ( $k$ ) is related to the soil modulus of elasticity ($E_s$) through a dimensionless parameter known as Winkler coefficient ($\delta$):

$$k = \delta . E_s \quad [8]$$

The pile head impedance functions for 2D substructure model are derived through an algebraic procedure which has been described in detail in Torabi (2016), and by applying appropriate boundary conditions to Eq. 6 and its derivatives representing bending moment and shear force. The resultant impedance matrix for a hinged-tip long pile with $\lambda L > 2.5$ is implicitly expressed in polynomial terms as follows (Pender 1993):

$$S_p = \begin{bmatrix} 4E_pI_p\lambda^3 & 2E_pI_p\lambda^2 \\ 2E_pI_p\lambda^2 & 2E_pI_p\lambda \end{bmatrix} \quad [9]$$

whereas, for a fixed-tip short pile with $\lambda L < 2.5$ , the impedance functions are represented by trigonometric functions (Mylonakis 1995) that must be expressed in polynomial form. Thus, infinite McLaurin series are employed in this study to accomplish this transform, as given below:

$$f(x) = \sum_{n=0}^{\infty} \frac{f^{(n)}(a)}{n!}(x-a)^n \quad [10]$$

After several steps of expanding functions and simplification, the polynomial representation of impedance functions can be written as:

$$\overline{S}_p = \begin{bmatrix} \frac{12E_pI_p}{L^3}\overline{\beta}_{uu} & \frac{6E_pI_p}{L^2}\overline{\beta}_{u\theta} \\ \frac{6E_pI_p}{L^2}\overline{\beta}_{u\theta} & \frac{4E_pI_p}{L}\overline{\beta}_{\theta\theta} \end{bmatrix} \quad [11]$$

where,

$$\begin{aligned} \overline{\beta}_{uu} &= (1 + 1.24\mathrm{E}^{-1}(\lambda L)^4 - 4.9\mathrm{E}^{-4}(\lambda L)^8) \\ \overline{\beta}_{u\theta} &= (1 + 3.5\mathrm{E}^{-2}(\lambda L)^4 - 2.1\mathrm{E}^{-4}(\lambda L)^8) \\ \overline{\beta}_{\theta\theta} &= (1 + 9.5\mathrm{E}^{-3}(\lambda L)^4 - 8.9\mathrm{E}^{-5}(\lambda L)^8) \end{aligned} \quad [12]$$

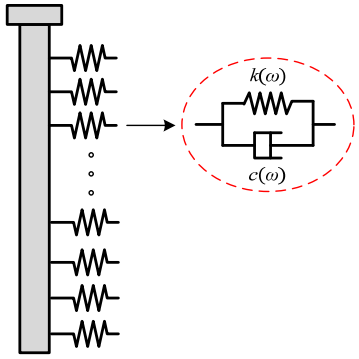


Figure 3. Visco-elastic Winkler model of soil-pile interaction

2.4. Derivation of Equivalent-linear Impedance

The average equivalent-linear (EL) pile subgrade impedance ($\bar{\lambda}$) is computed from rigorous results of continuum model following the proposed hybrid method. The idea is to first back calculate ($\bar{\lambda}$) from algebraic solution of the complex-valued force-deformation matrix in Eq. 2, and compute subsequently the corresponding pile head impedance functions for the three vibration modes. It should be noted that in reality, the Winkler coefficient ($\delta$) value is not constant along the pile length even for the piles in homogeneous linear elastic soil medium (Syngros 2004). Thus, varying $\delta$ values with depth is in contrast with the common assumption of a bed of uncoupled independent springs supporting the pile. Thus, approximating the realistic pile head impedances with inhomogeneous distribution of $\delta$ values by the closed-form impedances as a function of equivalent homogeneous wavenumber ($\bar{\lambda}$) is associated with some error that will be examined later in this paper.

The derivation procedure is based on solving Eq. 2 in which Fourier transforms of the prescribed force and recorded displacement vectors at the pile head are inserted from the finite element models. Depending on the pile tip boundary condition and the $\lambda L$ value, the corresponding impedance matrix with the polynomial elements (i.e. Eqs. 9 and 11) is adopted. The algebraic derivation procedure is described in the following for the case of a fixed-tip relatively short pile for which the approximating polynomial function should be used. This is related to the assumption that in such a case, upon pile-soil gap creation and degradation of soil stiffness under strong inertial structural loads, the $\bar{\lambda}L$ value is very likely to fall below $\lambda L = 2.5$, while in the case of a hinged-tip long pile or short fixed-tip pile under weak earthquake motion with larger $\bar{\lambda}L$ value, the asymptotic impedances (Eq. 9) can be used. As a representative back-calculation procedure, for a fixed-tip pile with $\bar{\lambda}L < 2.5$, the polynomial impedance matrix of Eq is used in Eq. 12 to derive $\bar{\lambda}$ as follows:

$$\begin{bmatrix} \frac{12E_pI_p}{L^3}\overline{\beta}_{uu} & -\frac{6E_pI_p}{L^2}\overline{\beta}_{u\theta} \\ -\frac{6E_pI_p}{L^2}\overline{\beta}_{u\theta} & \frac{4E_pI_p}{L}\overline{\beta}_{\theta\theta} \end{bmatrix} \begin{Bmatrix} \hat{u}_p \\ \hat{\theta}_p \end{Bmatrix} = \begin{Bmatrix} \hat{V}_p \\ \hat{M}_p \end{Bmatrix} \quad [13]$$

where it is evident that $\bar{\lambda}$ as the only variable that can be determined by solving each of the two equations in Eq. 13. But, the obtained value from one equation (i.e., force equilibrium) does not satisfy the other one (i.e., moment equilibrium), thus, these two equations must be solved simultaneously in order to interpolate an optimum $\bar{\lambda}$ value which can satisfy both equations with an acceptable error margin. The interpolation procedure has been fully described in Torabi (2016) for both types of the pile shaft.

3. Application examples and verification

The described hybrid computational procedure in the previous sections is applied to two practical cases including long hinged-tip and short fixed-tip large-diameter pile shafts subjected to static and dynamic loadings as shown in Fig.4. Results from static analyses are used to identify margin of error associated with interpolation of subgrade stiffness. A parametric study is performed using dynamic excitations with a range of loading frequency and amplitude to characterize frequency domain behavior of EL impedances. The analyses involve a single pile shaft with a diameter of $D_p$=2.3 m embedded in a homogenous soil continuum, with two different lengths of 15m and 30m to represent short rock socketed and long hinged-tip piles, respectively. Use of such a large diameter pile is intended to represent extended RC shafts recommended by Caltrans (2013) design guidelines for supporting bridges. The stress-strain behavior of the soil is modelled using linear elastic and elastoplastic soil models. Two types of soil-pile interface are considered: perfect rigid bonding and elasto-perfectly plastic contact elements. The linear elastic soil model and the rigid soil-pile interface bonding are used for the purpose of validating performance of the back-calculating method proposed in this study. Because, these modeling conditions are the assumptions underlying previous studies which suggest equations for the modulus of subgrade reaction. The pile model is assumed linear elastic with the flexural stiffness of $E_pI_p$=3.43×$10^5$MN.$m^2$ in all of the analyses in order to limit the system inelasticity effects on soil behavior. Table 1 presents elastic properties of the soil and pile used in pile head loading analysis.

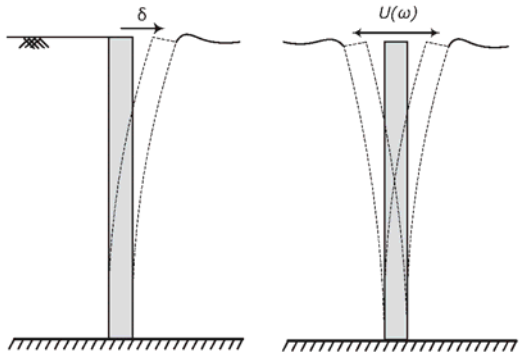


Figure 4. Schematic of static and dynamic pile head loading

Table 1. Input elastic parameters for the soil model

| Element | constitutive model | $V_s$ (m/s) | $G_r$ * | $E_r$ | $B_r$ | $S_u$(kPa) |
|---|---|---|---|---|---|---|
| Soil | linear elastic | 80 | 10.2 | 28.7 | 47.8 | — |
| | nonlinear inelastic | 130 | 27 | 75.7 | 126.2 | 45 |

$V_s$: shera wave velocity; G: Shear modulus; E: modulus of elasticity, B: Bulk modulus; $S_u$: Undrained shear strength

* "r" denotes small-strain value of the parameter (Mpa)

3.1. Static loading

In static analysis, the lateral displacement prescribed at the pile head is increased incrementally and the corresponding load at the pile head is recorded to identify the ultimate lateral pile resistance as well as the lateral bearing strength envelope of the pile. The static analysis begins with finite element simulation of soil-pile interaction in linear elastic soil and rigid interface bonding to evaluate the obtained equivalent modulus of subgrade reaction with the values given by existing expressions in literature. The equivalent wavenumber at zero frequency ($\bar{\lambda}_0$) is computed for the long hinged-base and short rock-socketed piles. Table 2 compares the FE-based normalized Winkler modulus ($\bar{\delta}$) with those given by the equation proposed by Syngros (2004), which is expressed as:

$$\delta = 3.5\left(E_p/E_s\right)^{-0.11} \quad [14]$$

Table 2. Verification of subgrade modulus

| Pile | Length | $V_s$ (m/s) | $E_p/E_s$ | $\hat{\delta}$ | $\delta_s$ |
|---|---|---|---|---|---|
| short Fixed-tip | 12 | 80 | 870 | 1.64 | 1.61 |
| long Hinged-tip | 30 | 130 | 330 | 1.49 | 1.78 |

$\hat{\delta}$: modulus from this study $\delta_s$ : Syngros (2004)

The static push over analysis is extended to a realistic interaction problem involving nonlinear soil and interface behavior to characterize degradation of the equivalent modulus of subgrade reaction and the corresponding head impedances with increasing imposed displacement at the pile head. In nonlinear analysis, the imposed displacement at the pile head is incrementally increased until the lateral resistance of the pile reaches failure state. The failure load is determined at loading increment where tangent stiffness equals to 1% of the initial value. Fig. 5 shows variation of the computed static normalized EL subgrade modulus with the pile head displacement ratio. The subgrade modulus is normalized with respect to the soil's modulus of elasticity ($E_s$) shown in Table 1. The pile head displacement (u)is also normalized by the parameter ($u_{50}$) denoting the displacement at which 50% of the failure lateral capacity of the pile is mobilized. As shown, almost 80% of the idealized elastic subgrade modulus is degraded due to pile-soil gap creation and inelastic soil behavior around the pile shaft before 50% of the lateral capacity is mobilized.

The error of subgrade interpolation is expected to increase in inelastic interaction where variation of the subgrade modulus along the pile length becomes progressively inhomogeneous due to inelastic soil and interface deformation. For evaluation of margin of this error, the pile head lateral force is reproduced at each lateral displacement increment by using the computed head stiffness ($\bar{k}_{uu}, \bar{k}_{u\theta}$), and compared with that from the continuum model as follows:

$$\overline{P}_H = \bar{k}_{uu}.u_p + \bar{k}_{u\theta}.\theta_p \quad [15]$$

$$\varepsilon_p(\%) = \frac{\overline{P}_H - P_H}{P_H} \quad [16]$$

where $\varepsilon_p$ denotes the estimation error in percent, $\bar{p}_H$ and $p_H$ denote the estimated and recorded pile head forces, respectively, which are compared schematically in Fig. 6. As expected, the failure lateral capacity of the short rock-socketed pile is larger than that of the long hinged-tip one due to contribution of the flexural stiffness of the pile's cross section. Fig. 6 also demonstrates variation of the estimation error with increasing imposed lateral displacement for the fully elastic rigid interface and the inelastic interactions of short fixed-tip and long hinged-tip piles. From the plot for elastic interaction, the estimation error solely due to the assumption of independent homogeneous Winkler spring is 5.6% and constant with the imposed displacement. For the inelastic cases, the error is shown to be influenced by the lateral pile performance such that in the 30m hinged-tip pile, the error progressively increases with increasing pile head displacement and approaches to an asymptotic value of about 10%, whereas in the 15m fixed-tip pile, the maximum error value of 10% is reached at much lower $u/u_{50}$ ordinate, thereafter, it decreases until reaching zero at $u/u_{50} = 2.5$. This is because the surrounding soil yields at smaller head displacement in the short pile, above which the pile's flexural stiffness dominates the lateral bearing capacity mechanism. For design purposes, it is important to identify the margin of error within the range of design load which is considered as 67% of the ultimate lateral resistance of a drilled pile shaft, according to AASHTO LRFD (2012) guidelines. The specified design load limits in Fig. 6 indicate corresponding $\varepsilon_p$ values of less than 10% for both the pile cases, which is an acceptable range of error.

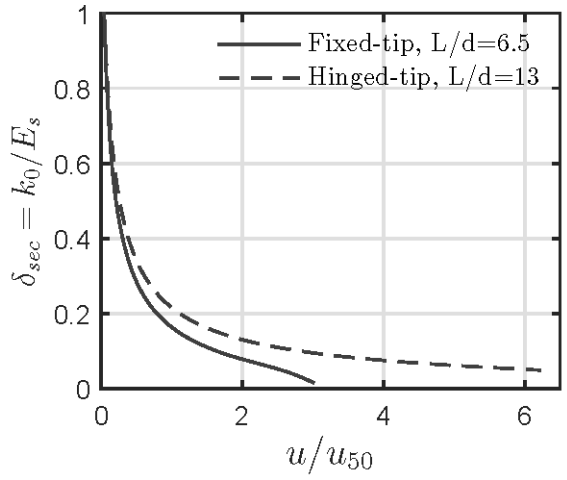


Figure 5. Computed degradation trend of the average subgrade stiffness under static pile head load

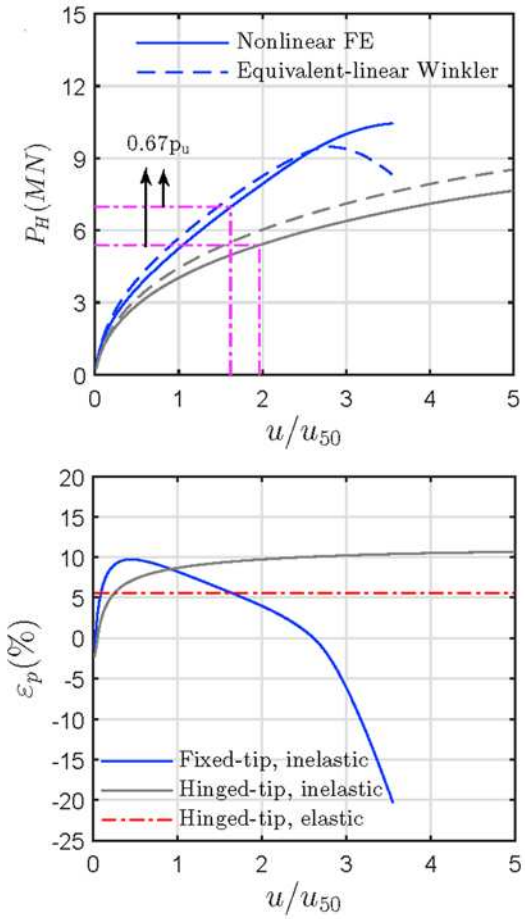


Figure 6. Comparison of the static pile head lateral force and the associated interpolation residual

3.2. Dynamic loading

The goal of this section is to characterize dynamic pile head impedance functions under the influence of soil and interface inelasticity. Focusing on derivation of the pile impedance functions, a massless pile is considered in numerical analysis of the pile with dynamic head loading to eliminate the effect of inertial forces in frequency response of the soil-pile system. In the cyclic mode, frequency content of the loading time history must sweep a wide-band frequency range to capture frequency-dependent characteristic of the soil-pile interaction. This excitation which is a sine sweep function is used to investigate linear elastic interaction, and also discriminate influence of the soil and interface nonlinearity over a broad range of frequency. The used linear chirp function covers a frequency range between 0.1 to 10 Hz within the duration of 10 seconds.

3.2.1 Effects of soil and interface inelasticity

The linear chirp excitation is prescribed at the pile head in order to distinguish the role of interface and soil nonlinearity on the interaction mechanism. The pile models are identical to those in static analysis, embedded in 15m and 30m soil deposits with $V_s$=130m/s on an elastic bedrock. The amplitude of the linear chirp excitation is 1cm in order to induce moderate level of soil inelasticity. Fig. 7 shows comparison of the subgrade modulus (real part) for the 30m hinged-tip pile while Fig.8 shows comparison of the dashpot coefficient (imaginary part) for the both pile cases. Both plots demonstrate the significant impacts of the soil and interface inelasticity on dynamic stiffness and damping characteristics of the pile. In Fig. 8(a), the computed damping coefficient for the fully elastic case is verified against the analytical plain-strain damping model proposed by Gazetas and Dobry (1984), with the equation as follows:

$$\frac{C_r}{4B\rho_s V_s} = \left\{1+\left[\frac{3.4}{\pi(1-\nu)}\right]^{5/4}\right\}\left(\frac{\pi}{4}\right)^{3/4} a_0^{-1/4} \qquad [17]$$

where B denotes the pile radius, $\rho_s$ and $V_s$ are the mass density and shear wave velocity of the soil, respectively, and $a_0$ denotes the dimensional frequency defined as $a_0 = 2\pi fB/V_s$. The comparison which demonstrates a good match between the two data is shown for only the frequency range of radiation damping existence. Because the computed damping is in the soil deposit on a rigid bedrock, as opposed to the model values that are for piles in semi-infinite elastic half space in which the damping value yields to infinity at very low frequencies.

As shown in both plots of Fig. 8, the linear elastic soil assumption leads to a noticeable overestimation of subgrade modulus and damping coefficient even under small displacement amplitude. Moreover, it causes large oscillation (peaks and valleys) at the characteristic frequencies of the soil-pile system. Basically, the frequency-domain variation of the stiffness and damping of any SSI problem in shallow soil deposit over rigid bedrock exhibits undulation (Gazetas 1983,1984). This is resulted from resonance between the natural frequencies of the soil standing wave due to multiple reflection at bedrock and ground surfaces. As a result, vibrating foundation emanates larger amount of energy to the soil domain (radiation damping) with smaller resistance by the surrounding soil. In the case of this study, the valleys exhibited by the stiffness and the peaks by the damping are found to occur at two characteristic frequencies of the system. The first one ($a_0 \approx 0.18$), which is shown to be identical between the two sites (15m, 30m) and the pile types, is the frequency of the soil-pile characteristic wavelength frequency, given by $\omega_\lambda = Re(\bar{\lambda}_\omega)V_s$. This frequency is a function of soil-pile relative stiffness parameter or characteristic wavenumber ($\lambda$) which controls attenuation of the dynamic excitation along the pile shaft and the soil shear wave velocity. The second one, which varies between the two soil deposits, is almost twice the first natural site period. Thus, it can be concluded that the resonance occurs probably at the second modal frequency of the soil deposit over rigid bedrock. In overall, variation of the stiffness and damping exhibits fairly smooth trend without large spikes when inelastic soil and interface deposit and the loading frequency, rendered by the actions are allowed in the system.

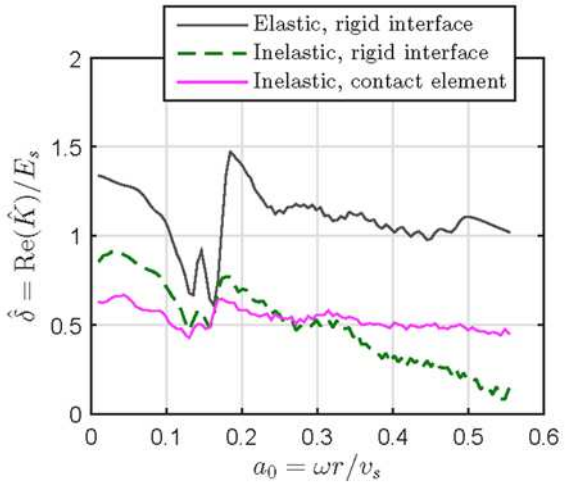


Figure 7. Effect of soil and interface inelasticity on the subgrade dynamic stiffness

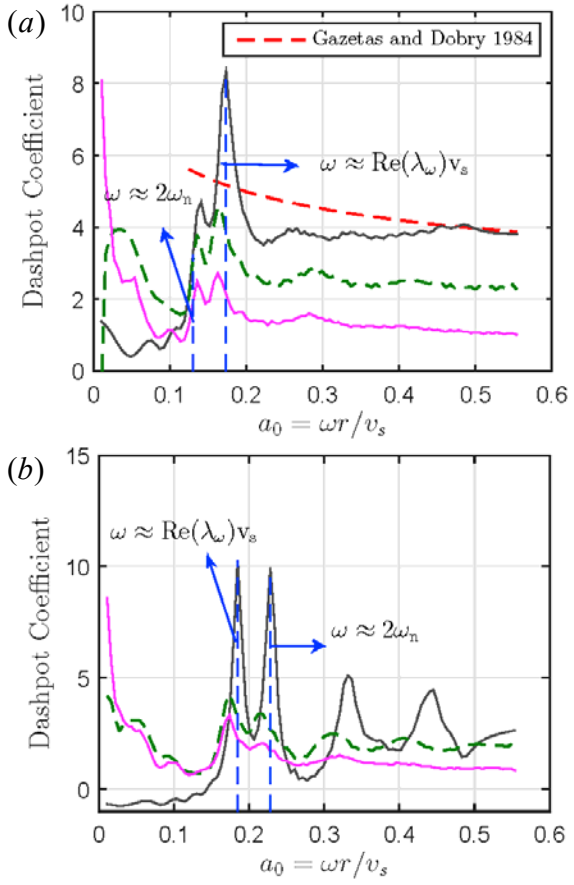


Figure 8. Effect of soil and interface inelasticity on the subgrade damping a) 30m hinged-tip, b) 15m fixed-tip pile

In order to explore the effects of inelasticity on the pile head impedances, Fig. 9 compares the computed horizontal dynamic stiffness and damping ratio of the pile head for the fixed-tip short pile, as a representative impedance mode. The computed parameters are defined in normalized form to be consistent with the reference solutions in literature, which are expressed for a representative horizontal mode as follows:

Dynamic stiffness: $\mathrm{Re}(\hat{K}_{uu})/E_s d$

Damping ratio: $\mathrm{Im}(\hat{K}_{uu})/2\,\mathrm{Re}(\hat{K}_{uu})$

where $\hat{K}_{ij} = k_{ij} + ic_{ij}\omega$ denotes the impedance function, $E_s$ and $d$ denote Young modulus of the soil and the pile diameter, respectively. In both plots, the damping ratio of the inelastic soil with rigid soil-pile interface is shown to be notably overestimated in the frequency range where radiation damping is dominant. This indicates that the hysteretic damping is significantly overestimated by the rigid interface despite the adverse impact of the soil inelasticity on radiation damping. Moreover, these two plots demonstrate frequency range for the active damping mechanisms. As shown, the natural site frequency of the shear wave which corresponds to $a_0$=1.2 in Fig. 9 is the cut-off frequency for the radiation damping, below which, the vibrating pile is unable to emanate waves into the soil domain, and the frequency-independent hysteretic damping is the only acting dissipation mechanism. This is observed by comparing the damping trend of the inelastic and elastic soils. Such an observation was also reported by Gazetas (1984), but with a difference that in his work a huge jump of damping ratio occurs at the first natural site frequency for the shear wave, whereas, such a rise is observed at the characteristic frequency of $\omega_\lambda$ or the modal site frequency for the standing waves in the soil domain, whichever is smaller.

(a)

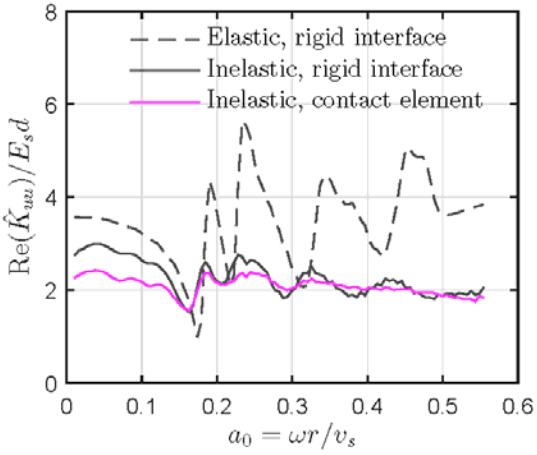

(b)

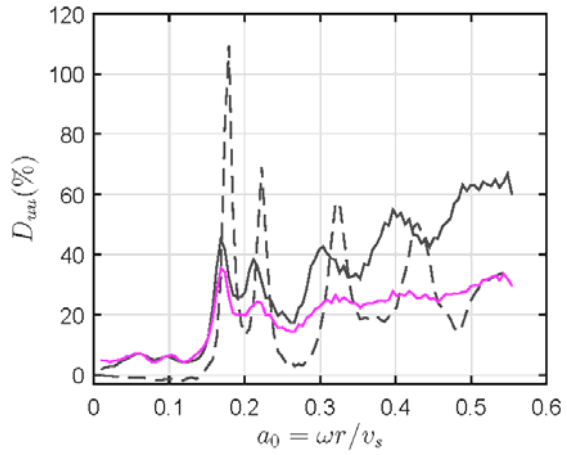


Figure 9. Effect of soil and interface inelasticity on the horizontal pile head impedance for 15m fixed-tip pile

## 4. Conclusion

In this paper, a summary of the hybrid analytical-numerical method was presented, which is devised to improve accuracy of the substructure analysis for inelastic SPSI problems. The idea was to approximately calibrate the coefficients for the average visco-elastic Winkler support of pile shaft using the rigorous results from continuum model. Representative results from applying the proposed method to static and dynamic pile loadings were presented.

Computed subgrade stiffness trend from static analysis indicated that a large part of the lateral stiffness loss is caused by the gapping between soil and pile. It was also shown that the back-calculated average subgrade stiffness can reproduce the pile head lateral force with the maximum error of 10%. The back-calculated subgrade impedances from sine sweep excitation of the pile head indicated significant impact of the soil and interface inelasticity on the reduction of pile head impedances, in particular suppression of the radiation damping level.

## 5. References


AASHTO. 2012. *LRFD Bridge Design Specifications*: American Association of State Highway and Transportation Officials, Washington D.C., USA.

Caltrans. 2013. *Seismic Design Criteria, version 1.7,* California Department of Transportation.

Gazetas, G. 1983. Analysis of machine foundation vibrations: state of the art. *International Journal of Soil Dynamics and Earthquake Engineering, 2*(1), 2-42.

Gazetas, G. 1984. Seismic response of end-bearing single piles. *International Journal of Soil Dynamics and Earthquake Engineering, 3*(2), 82-93.

Gazetas, G., & Dobry, R. 1984. Simple radiation damping model for piles and footings. *Journal of Engineering mechanics, 110*(6), 937-956.

Gazetas, G. 1991. *Foundation vibrations: foundation engineering handbook 2nd edition*. Y. Fang, ed., Van Nostrand Reinhold, New York, N.Y., 553-593.

Kausel, E., Whitman, R. V., Morray, J. P., & Elsabee, F. 1978. The spring method for embedded foundations. *Nuclear Engineering and Design, 48*(2), 377-392.

Makris, N., Badoni, D., Delis, E., & Gazetas, G. 1994. Prediction of observed bridge response with soil-pile-structure interaction. *Journal of Structural Engineering, 120*(10), 2992-3011.

McGann, C. R., Arduino, P., & Mackenzie-Helnwein, P. 2011. Applicability of conventional py relations to the analysis of piles in laterally spreading soil. *Journal of Geotechnical and Geoenvironmental Engineering, 137*(6), 557-567.

McKenna, F., Fenves, G. 2001. *The OpenSees command language manual, Version 1.2*: Pacific Earthquake Engineering Research Center, University of California, Berkeley, CA. http://opensees.berkeley.edu.

Mylonakis, G. 1995. *Contributions to static and seismic analysis of piles and pile-supported bridge piers.* PhD Thesis, State University of New York at Buffalo.

Mylonakis, G., & Gazetas, G. 2000. Seismic soil-structure interaction: beneficial or detrimental? *Journal of Earthquake Engineering, 4*(03), 277-301.

N. NIST. Soil-Structure-Interaction for Building Structures (NIST GCR 12-917-21). National Institute of Standards and Technology, Gaithersburg, MD 20899, September 2012.

Novak, M. 1974. Dynamic stiffness and damping of piles. *Canadian Geotechnical Journal, 11*(4), 574-598.

Pender, M. 1993. Aseismic pile foundation design analysis. *Bulletin of the New Zealand National Society for Earthquake Engineering, 26*(1), 49-160.

Petek, K. A. 2006. *Development and application of mixed beam-solid models for analysis of soil-pile interaction problems.* PhD Thesis, University of Washington.

Rahmani, A., Taiebat, M., Finn, W. L., & Ventura, C. E. 2016. Evaluation of substructuring method for seismic soil-structure interaction analysis of bridges. *Soil Dynamics and Earthquake Engineering, 90*, 112-127.

Syngros, K. C. 2004. *Seismic response of piles and pile-supported bridge piers evaluated through case histories.* PhD Thesis, The City University of New York.

Torabi, H. 2016. *A hybrid appraoch for inelastic soil-strcutrue interaction analysis of pile-supported bridges*. PhD thesis, Carleton University, Ottawa, Canada

Varun, Assimaki, D., & Gazetas, G. 2009. A simplified model for lateral response of large diameter caisson foundations—Linear elastic formulation. *Soil Dynamics and Earthquake Engineering, 29*(2), 268-291.

Zhang, J., & Makris, N. 2002. Kinematic response functions and dynamic stiffnesses of bridge embankments. *Earthquake Engineering & Structural Dynamics, 31*(11), 1933-1966. doi:10.1002/eqe.196

Wolf, J. P. (1985). *Dynamic soil-structure interaction*: Prentice Hall, Englewood Cliffs, N.J.